JAST, Vol. 6, No. 1, pp 25–35

JAST
Journal of Aerospace Science and Technology

Impact of Body on the Tail Surface Flowfield at High Incidences

A. R. Davari[1], M. Hadi Dulabi[2], M. R. Soltani[3], F. Askari[4]

An experimental study was performed to investigate the effects of the body angle of attack on the tail surface pressure distribution for a half body-tail combination in subsonic flow. The results show, in small deflection angle regions, the tail deflection has the same effect on the surface pressure as the body angle of attack. However, at moderate to high deflections, the flowfiled caused by the tail deflection angle is completely different from that of the body angle of attack, which is an indication of the nose and body vortex shedding effects on the tail at a high angle of attack regime.

NOMENCLATURE

c	Tail chord at root section
b	Tail semi span
x/c	Dimensionless Chordwise distance measured from the tail leading edge
y/b	Dimensionless spanwise distance measured from the body surface
α	Body Angle of attack with respect to the oncoming flow
δ	Tail deflection angle with respect to the body
c_p	Pressure coefficient
C_N	Tail normal force coefficient

INTRODUCTION

The aerodynamic of aircraft at high angles of attack is a subject being pursued diligently because the modern agile fighter aircraft and many of the current generation of projectiles must be able to continue their flight when operating in the vicinity and beyond stall angles of attack. Much of the past and present research and development efforts in aerodynamics are devoted to investigations of the numerous flow phenomena, which are accentuated as the angle of attack of complex configurations reaches the stall level and beyond.

In an aircraft or projectile, the interference problem among the components is of great importance. For the tail-control flying vehicles, the increasing need towards flying at high angles of attack without losing the vehicle controllability requires employing more effective tails. For body-tail configurations, it is desirable to obtain a certain amount of lift with an acceptable ratio of the tail deflection angle to the body angle of attack, δ/α.

Many theoretical works were performed to study the role of the lee side vortices on the aerodynamic behavior of the bodies of revolution in the low speed subsonic flow at high angles of attack [1-3]. Grosche [4] has shown that the lee side vortices on the body are strongly affected by both the wing downwash and the wing sweep angle.

The influence of high-angle-of-attack aerodynamic phenomena on aircraft and projectile static and dynamic stability characteristics is the topic of several recent AGARD lecture series [5,6]. Of particular interest are the studies dealing with asymmetric body vortical flows and vortex breakdown. Each of these phenomena can affect the dynamic behavior of a projectile as it executes a high-angle-of-attack maneuver.

In the case of either an aircraft having a long slender forebody or a high fineness ratio projectile, the forebody vortices can become asymmetric as the angle of attack is increased. The asymmetric disposition of the vortices gives rise to a significant side force and

1. *Assistant Professor, Dept. of Mech. and Aerospace Eng., Science and Research Campus, Islamic Azad Univ., Tehran, Iran.*
2. *Assistant Professor, Dept. of Aerospace Eng., Malek Ashtar Univ., Tehran, Iran.*
3. *Professor, Dept. of Aerospace Eng., Sharif Univ. of Tech., Tehran, Iran.*
4. *Graduate Research Assistant, Sharif Univ. of Tech., Tehran, Iran.*

yawing moment resulting from the flow asymmetry. The problem can become more complicated if the asymmetric vortex wake interacts with the aft lifting surfaces such as wings or tail that amplifies the lateral forces and moments.

Hunt [7] summarized the asymmetric vortex wakes and their associated forces and moments. He clearly determined what is known and what remains to be understood regarding the asymmetric vortex wakes. His studies revealed that the asymmetric vortex wake is extremely sensitive to free-stream turbulence, geometric asymmetries, nose geometry, and Reynolds number. It appears that the maximum asymmetric load occurs when the boundary layer flow is either completely laminar or completely turbulent. Based on the experimental studies, Lamont [8] found that if the boundary layer is transitional, one can usually expect to find the lowest vortex-induced side forces.

Another aerodynamic problem that occurs at high angles of attack is the phenomenon known as vortex breakdown. As the angle of attack increases, the body or wing leading-edge vortices undergo a dramatic change. The axial velocity within the vortex diminishes, the vortex diameter increases, and the circumferential velocity decreases [9]. This sudden change in the vortex structure is called vortex breakdown or vortex burst.

One of the main applications of the existing knowledge on high alpha aerodynamics is in the engineering codes that are capable of predicting the aerodynamic forces and moments in a minimum time. Abney [10] has examined the well-known Missile Datcom engineering code for a high angle of attack range, and has shown that the wing-body and wing-tail interference factors are successfully estimated for standard body, fin, and body-fin configurations up to high angles of attack.

The attempts made so far were mainly concentrated on determining the wing- body-tail interference effects by either calculating the aerodynamic forces or flow visualization techniques. This is essentially helpful in developing some relations to take care of these effects when calculating the aerodynamic forces and moments of a body operating at the angles of attack well beyond stall.

In this paper, a comprehensive experimental study is conducted to obtain a physical insight into the impact of the body on the tail surface flowfiled. The effect of body angle of attack on the tail surface pressure distribution has been studied and compared with that of the tail deflection angle.

MODEL AND EXPERIMENTAL APPARATUS

The experiments were performed in an 80 by 80 cm subsonic wind tunnel at a constant velocity of 90 m/sec. The model was a semi body-tail configuration. 64 small pressure tabs were carefully drilled on both the upper

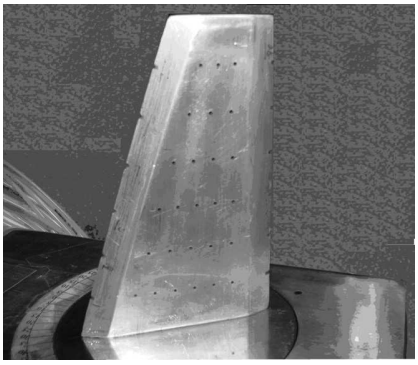

(a)

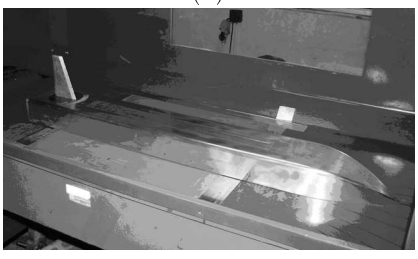

(b)

Figure 1. Model of the half body-tail configuration, (a) Tail surface pressure tabs (b) The model installed in the test section.

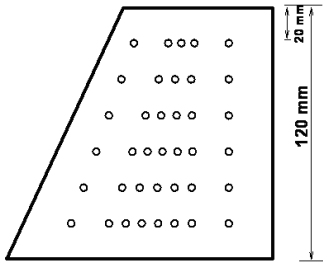

Figure 2. Schematic of the pressure tabs positioning on the upper surface.

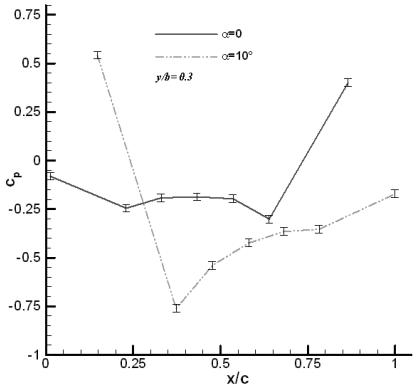

Figure 3. Typical measurement uncertainties on the tail upper surface.

and the lower surfaces of the tail. The tail sweep angle was about 20 degrees, and the experiments consisted of measuring the tail surface pressure distribution using sensitive pressure transducers for several combinations of the body angle of attack and the tail deflection angle. Figure 1 shows the pressure tabs on the tail and the model installed inside the test section. Geometric arrangement of the pressure tabs is shown in Figure 2. A vertical (spanwise) spacing of about 15 mm, and a horizontal (chordwise) spacing of about 7 mm were considered for the pressure tabs on the tail upper surface. However, the chordwise clearance of the first and the last pressure tabs near the leading edge and the trailing edge are different from the other tabs.

Two types of differential pressure sensors were used in the present experiments; 143PC05D and 143PC01D. One having a measuring range of ±5 psi was used for the front portion of the tail, and the other with a range of ±1 psi was used for the rear portion where the pressure gradient deceases.

An analytical approach [11] was used to estimate the errors involved in the pressure measurements. Both the single sample precision and the bias uncertainty in the pressure measurement were estimated. On this

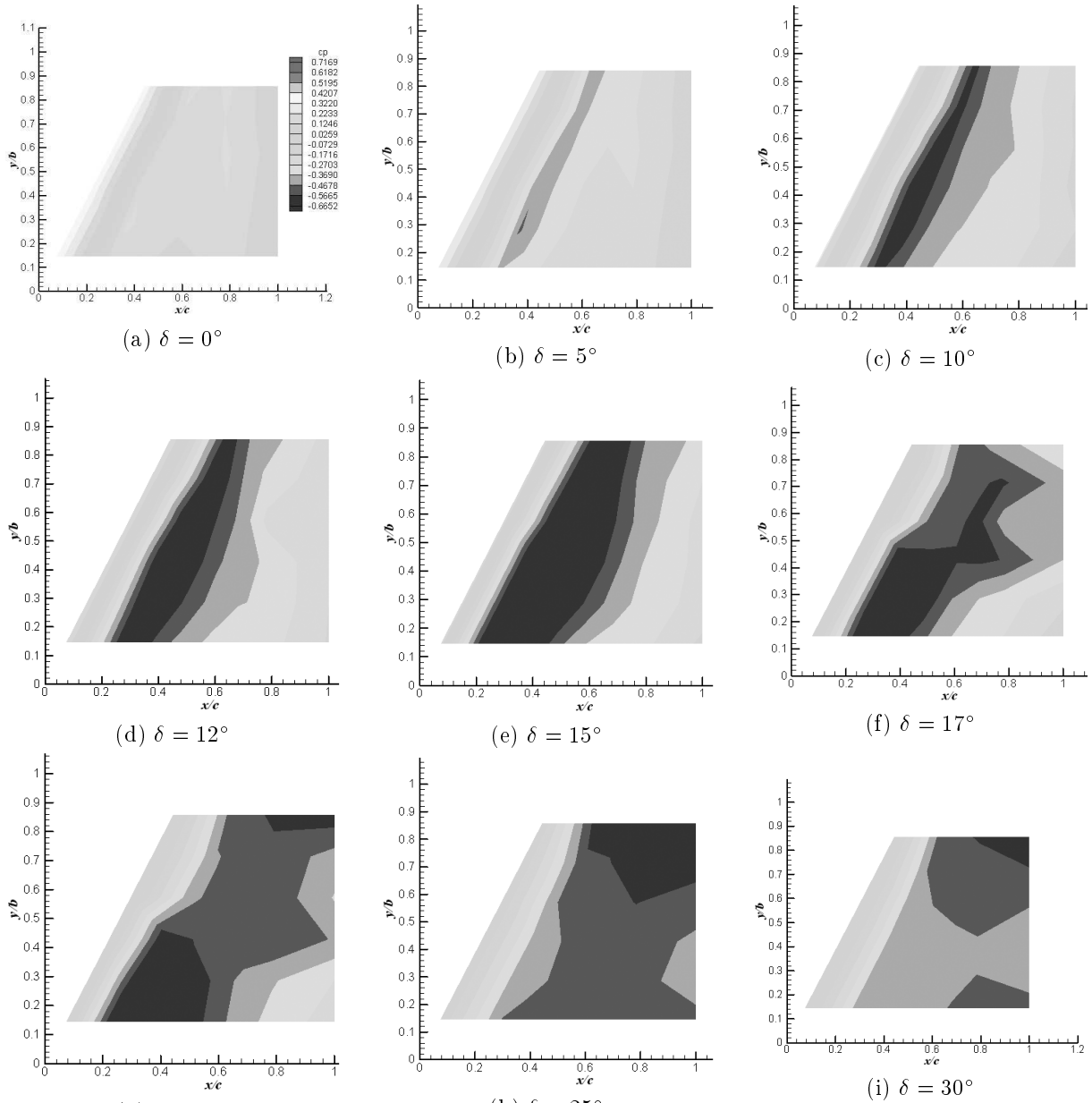

(a) $\delta = 0°$ (b) $\delta = 5°$ (c) $\delta = 10°$

(d) $\delta = 12°$ (e) $\delta = 15°$ (f) $\delta = 17°$

(g) $\delta = 20°$ (h) $\delta = 25°$ (i) $\delta = 30°$

Figure 4. Tail pressure contours at various deflection angles ($\alpha = 0$).

basis, the overall uncertainty for the presented data was found to be less than ±%3. Figure 3 shows a typical measurement uncertainty.

DISCUSSION

Figure 4 shows the development of the vortex-like flow on the tail as the tail deflection angle increases while the body angle of attack is fixed at zero. Note that the vortical flow pattern first appears near $\delta = 5°$, spreads over the surface towards the trailing edge, and starts to burst at about $\delta = 17°$. At this deflection angle, the vortical flow has been destroyed at the tail outboard region, while the inboard region is still dominated by the vortex. From $\delta = 17°$ to $\delta = 30°$ the burst region gradually covers the whole tail surface.

The chordwise pressure distribution at two spanwise sections; $y/b = 0.3$ and $y/b = 0.7$ at zero angle of attack of the body for different tail deflection angles are shown in Figure 5. Both Figures 5(a) and 5(b)

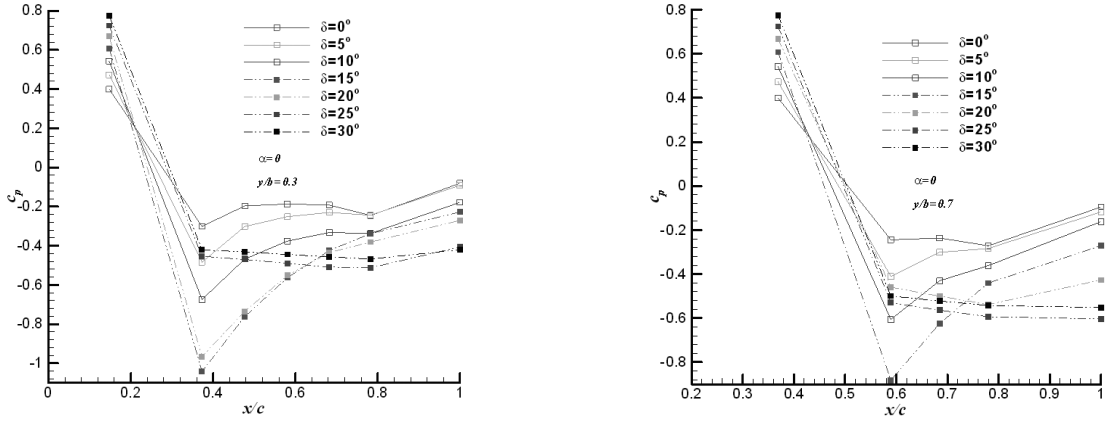

(a) $y/b = 0.3$ (b) $y/b = 0.7$

Figure 5. Effects of tail deflection on the spanwise pressure distribution ($\alpha = 0$).

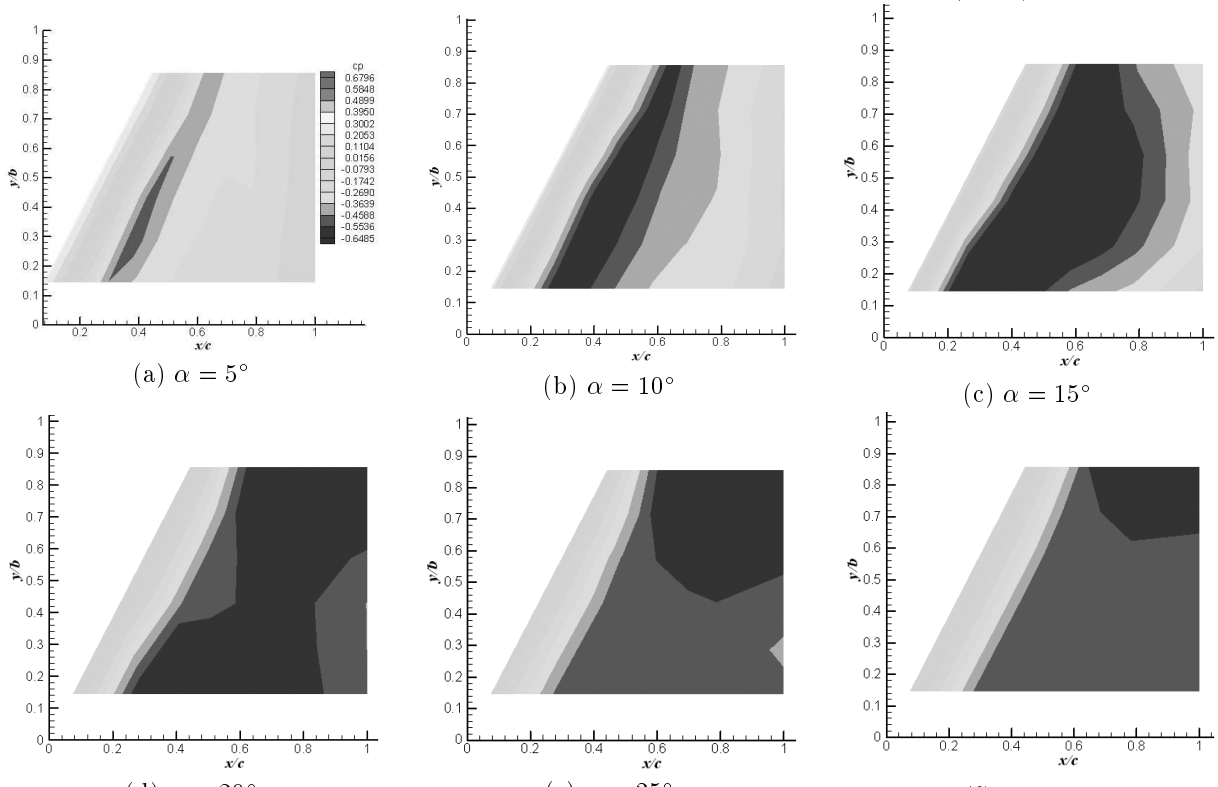

(a) $\alpha = 5°$ (b) $\alpha = 10°$ (c) $\alpha = 15°$

(d) $\alpha = 20°$ (e) $\alpha = 25°$ (f) $\alpha = 30°$

Figure 6. Tail pressure contours at various body angles of attack ($\delta = 0$).

show that the vortical flow is increased in strength and size up to about $\delta = 15°$ beyond which, the breakdown process starts and the amount of suction on the upper surface decreases. The relatively flat region on the chordwise pressure distribution for $\delta > 20°$ indicates that nearly 60% of the wing is covered by the burst vortex. Note that the vortex at the outboard region for $\delta = 20°$ is completely burst while the inboard portion is still dominated by this vortex.

The impact of the body on the tail flow pattern is shown in Figure 6, where the vortex development for zero tail deflection is shown as the body angle of attack increases. From Figures 6 and 7, it is evident that the pressure distribution over the tail varies only with the angle of attack, and is independent of the flow structure over the body for small to moderate body or tail angles up to about 10°. Within the small to moderate deflection angle range, this means that the surface pressure distribution over the tail remains unaffected, if either the body is set to $\alpha \leq 10°$ at zero tail deflection or the tail is deflected up to 10° at zero body angle of attack. This implies that within the small to moderate angle range, no remarkable viscous effect is observed in the flow behavior, and the flowfiled over the body does not affect the tail surface pressure distribution. In this situation, the body angle of attack at zero tail deflection and the tail deflection at zero body angle of attack both have an equivalent effect on the aerodynamic forces and moments developed on the tail.

For higher angles, the tail deflection angle and the body angle of attack are shown to have a different effect on the tail flow filed even though the net tail incidence referenced to the free stream remains constant.

This is clearly seen in Figure 7, where the pressure distribution at two spanwise sections $y/b = 0.3$ and 0.7 are shown. At low to moderate angles, both Figures 7(a) and 7(c) show that changing the body angle of attack is more efficient than the tail deflection angle in the sense that the suction peak is higher for the case where the body angle of attack changes at zero tail deflection. At 15 degrees deflection angle, where the vortex starts to breakdown, according to Figures 4 and 5, this behavior is different. Near the leading edge, the suction peak associated with the tail deflection is higher than that due to the body angle of attack while

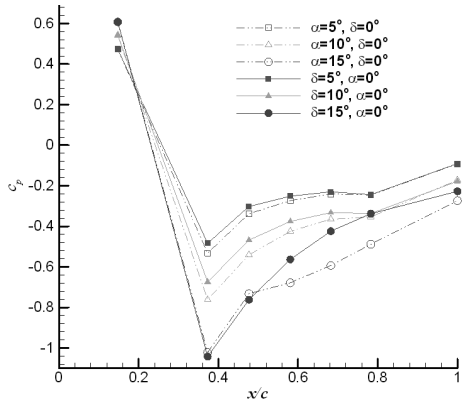

(a) $y/b = 0.3$, low to moderate angles

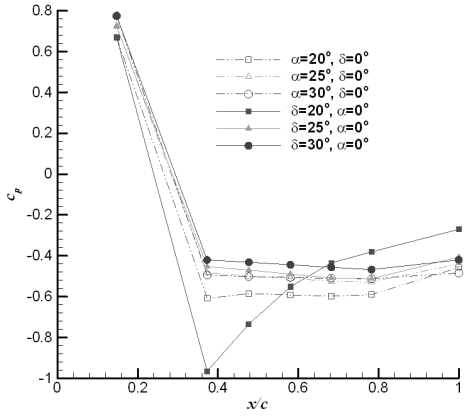

(b) $y/b = 0.3$, moderate to high angles

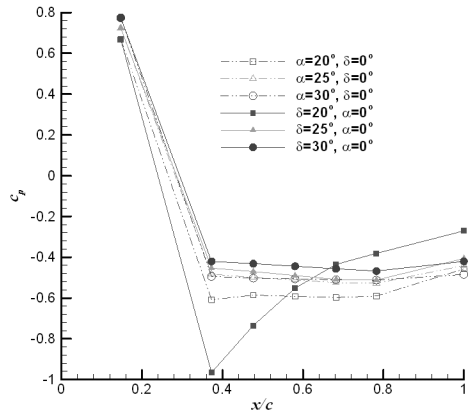

(a) $y/b = 0.7$, low to moderate angles

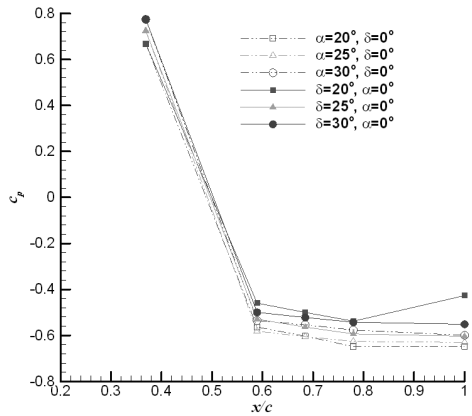

(b) $y/b = 0.7$, moderate to high angles

Figure 7. Comparison of the body angle of attack and the tail deflection effects on the tail spanwise pressure distribution.

for the rest of the section, the body angle of attack again appeares to be more effective.

For the high angle region of this figure, *i.e.*, Figures 7(b) and 7(d), as stated earlier, the effects of both the body and the tail deflection angles are shown to differ from each other significantly. For a 20 degree angle, the inboard sectional pressure possesses a lower suction peak for the body angle of attack than that for the tail deflection. Returning to Figures 4 and 6, for the tail deflection case, a relatively strong vortex is still observed at the inboard section at $\delta = 20°$, while this region for the body angle of attack case shown in Figure 6, nearly disappears. This is due to the nose and body vortices at high angles of attack, which are shed into the downstream region affecting the tail flow filed. For high deflection angles, once the whole surface is dominated by the burst flow, the more favorable effect of the body angle of attack in comparison to that of the tail deflection is observed again. It seems that the shed vortices from the nose and the body have a different effect on the tail flowfield at moderated angles where the tail vortex starts to burst, and at high angles where the burst flow covers the entire tail surface. Note from both Figures 7(b) and 7(d) at high angles that increasing the body angle of attack at zero tail incidence also decreases the adverse pressure gradient,

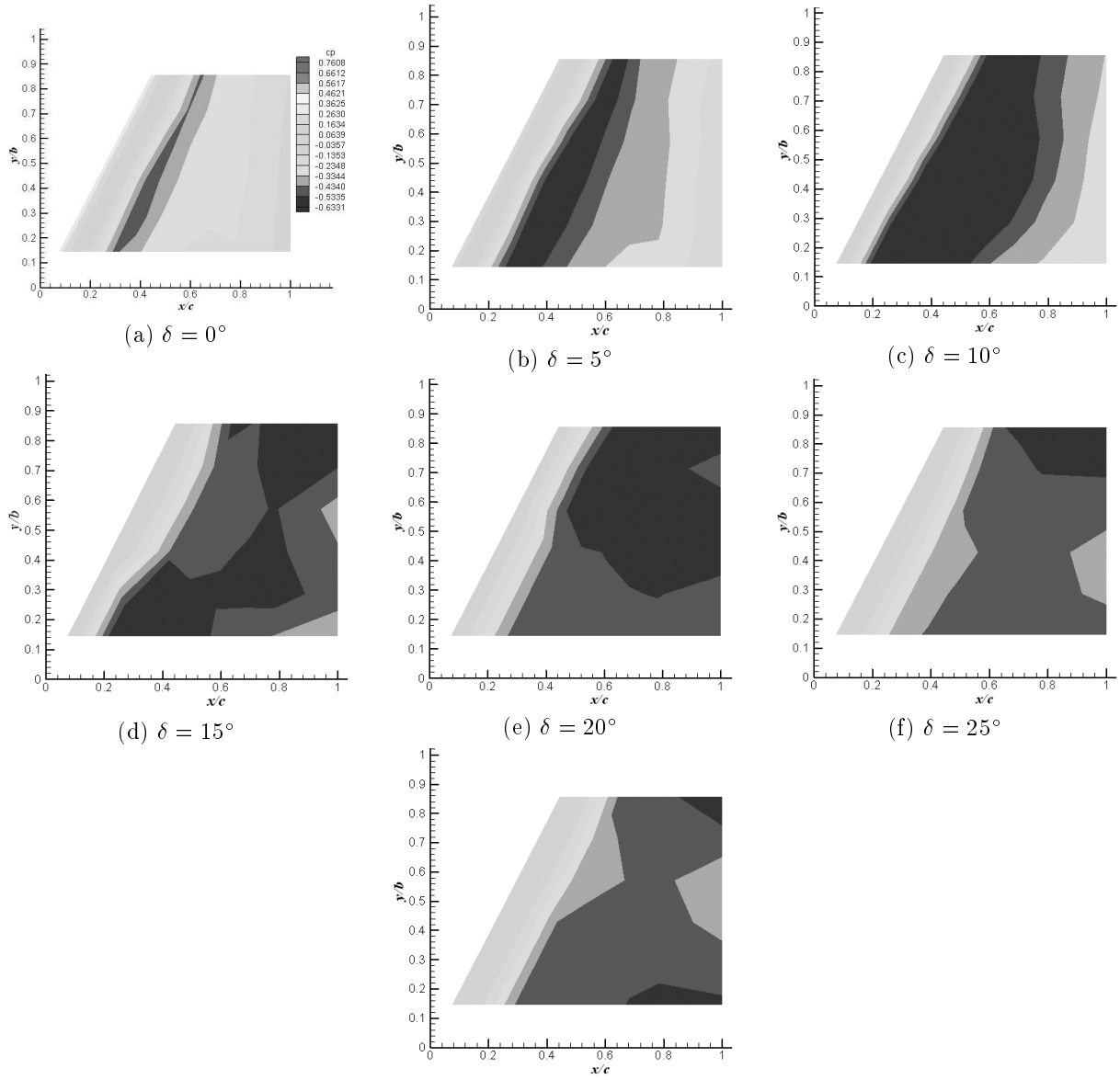

(a) $\delta = 0°$ (b) $\delta = 5°$ (c) $\delta = 10°$

(d) $\delta = 15°$ (e) $\delta = 20°$ (f) $\delta = 25°$

(g) $\delta = 30°$

Figure 8. Effects of tail deflection on the pressure contours ($\alpha = 5°$).

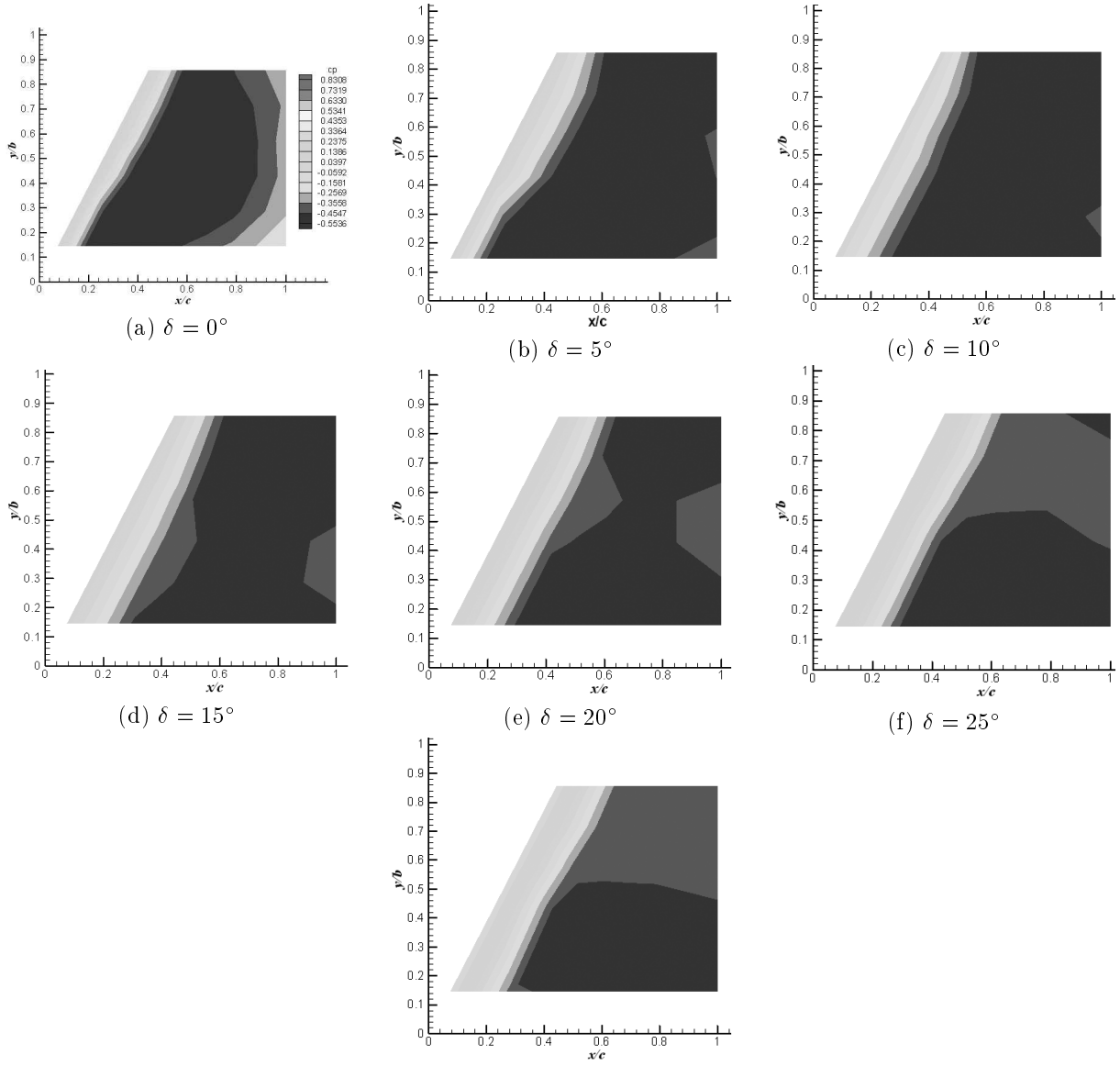

(a) $\delta = 0°$ (b) $\delta = 5°$ (c) $\delta = 10°$

(d) $\delta = 15°$ (e) $\delta = 20°$ (f) $\delta = 25°$

(g) $\delta = 30°$

Figure 9. Effects of tail deflection on the pressure contours ($\alpha = 15°$).

inhibiting the flow separation induced by the vortex burst.

Figures 8 and 9 show the tail surface pressure field for the two different body angles of attack of 5 and 15, respectively as the tail deflection angle increases. Comparing these two figures with Figure 4 at zero angle of attack, the effect of the combination of the body and the tail inclination angles on the tail effective angle is revealed with respect to the free stream. At 5 degrees body angle of attack and zero tail incidence (Figure 8(a)), the flowfield is nearly the same as that observed in Figure 4(b) at zero body angle of attack and a 5-degree tail incidence, as could be expected. This correspondence can be observed at higher angles, say $\alpha = 5°$, $\delta = 5°$ in Figure 8(b) with $\alpha = 0$, $\delta = 10°$ in Figure 4(c) or $\alpha = 5°$, $\delta = 10°$ in Figure 8(c) with $\alpha = 0$, $\delta = 15°$ in Figure 4(e). At 5 degrees body angle of attack in Figure 8, and for similar tail geometric angles, it seems that the low pressure region of the tail is more stretched on the surface, compared to the zero body angle of attack case seen in Figure 4. This difference is more pronounced at higher body angles of attack shown in Figure 9. The surface pressure at $\alpha = 15°$, $\delta = 0°$ in Figure 9(a) is not similar to that of $\alpha = 0$, $\delta = 15°$ in Figure 4(e), even though the tail net angle of attack for both cases is 15 degrees. The same is true for the other angles shown in Figures 9(b) and 4(g), 9(c) and 4(h), 9(d) and 4(i). The common

difference is the shape and the distribution of the low pressure or suction region on the tail at different body angles of attack and equal tail effective angles. This is due to the body and nose vortices effects on the tail flow especially at moderate to high angles of attack.

Figure 10 shows the different combinations of the body angle of attack and the tail incidence such that the net tail incidence with respect to the free stream is -5 degrees. Here the pressure contours for the lower surface are shown. As stated earlier, since the net tail angle is the same for the cases shown, one might expect that the pressure contours are the same. However, the cases in Figures 10(a) thorough 10(f) are not the same and this difference is obviously in the width of the suction region. As the body angle of attack increases, the width of this low pressure zone is also increased, even though the tail deflection balances the net inclination angle of the tail, setting it to -5 degrees constant for all cases. Similar behavior is seen in Fig. 11 for a net tail deflection of -15 degrees. Again, the contours are for the lower surface pressure.

As the absolute values of the body and tail inclination angles increase, the vortex breakdown point, first observed in Figure 11(b), moves spanwise towards the tail root, exposing more area on the tail to the bust flow. This shows that the absolute values of the body and the tail angle of attack, in the regions of vortex formation and break down, are more important than their combinational effect on the tail deflection angle with respect to the oncoming flow.

Figures 12 and 13 show the chordwise pressure distribution for the cases observed in the Figures 10 and 11. For the net tail deflection of -5 degrees on the lower surface, as the absolute values of both the body and tail angles increase, the vortical flow region on the tail flattens, extending between $x/c = 0.37$ and $x/c = 0.79$. This can effectively displace the tail center of pressure, and play an important role in the stability attitude of the vehicle though it seems that the resultant normal force is not changed significantly at the tail incidence of -5 degrees. The flowfield at a tail incidence of -5 degrees is shown in Figure 12. As seen in Figure 4, the vortex burst on the tail starts at about 15 degrees incidence. Thus, at this tail inclination angle, the pressure distribution on the tail remains more or less unchanged as the absolute values of the body and the tail deflections increase up to 15 degrees angle of attack of the body. At this angle of attack, the suction peak is decreased, indicating that the nose/body vortex shedding has promoted the vortex burst onset and the consequent flow separation on the tail surface.

Figure 14 shows the combinational effects of the tail deflection and the body angle of attack. Similar patterns are observed for $\alpha = 0$, $\delta = 5^\circ$ and $\alpha = 5^\circ$,

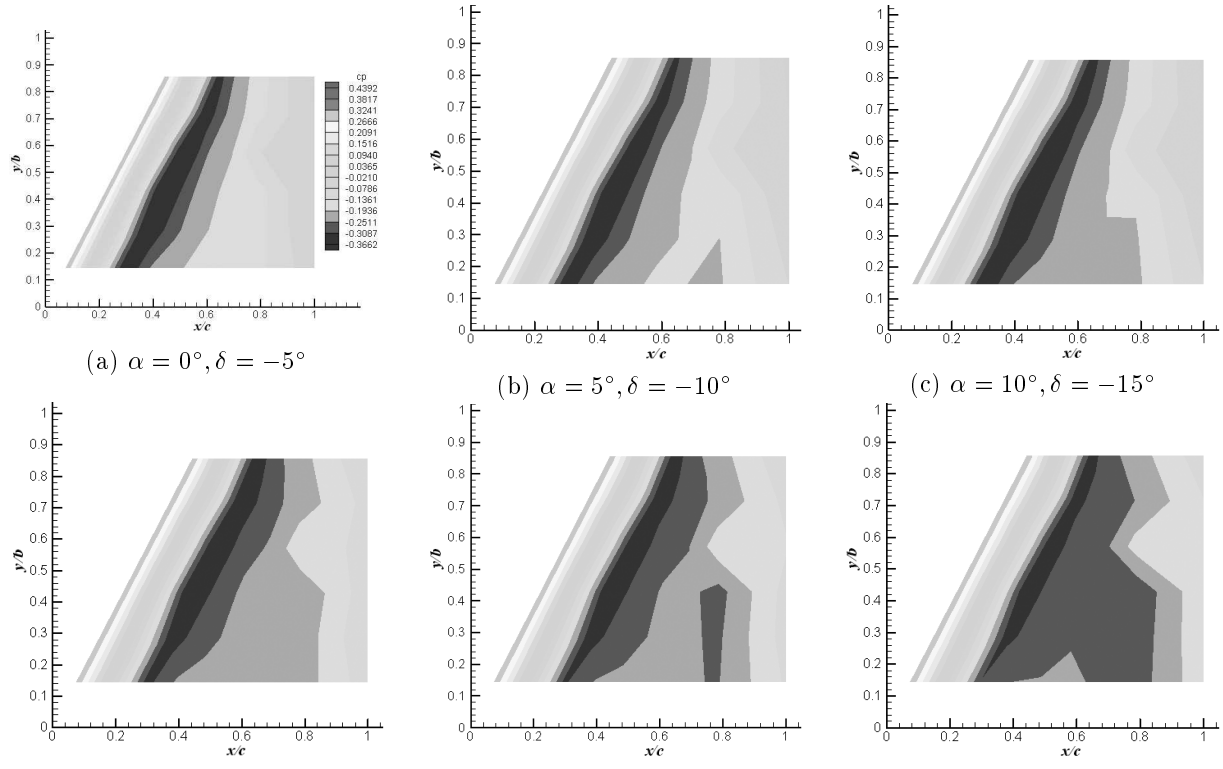

(a) $\alpha = 0^\circ, \delta = -5^\circ$ (b) $\alpha = 5^\circ, \delta = -10^\circ$ (c) $\alpha = 10^\circ, \delta = -15^\circ$

(d) $\alpha = 15^\circ, \delta = -20^\circ$ (e) $\alpha = 20^\circ, \delta = -25^\circ$ (f) $\alpha = 25^\circ, \delta = -30^\circ$

Figure 10. Tail pressure contours for combinations of body angle of attack and tail deflections for a net inclination of -5°.

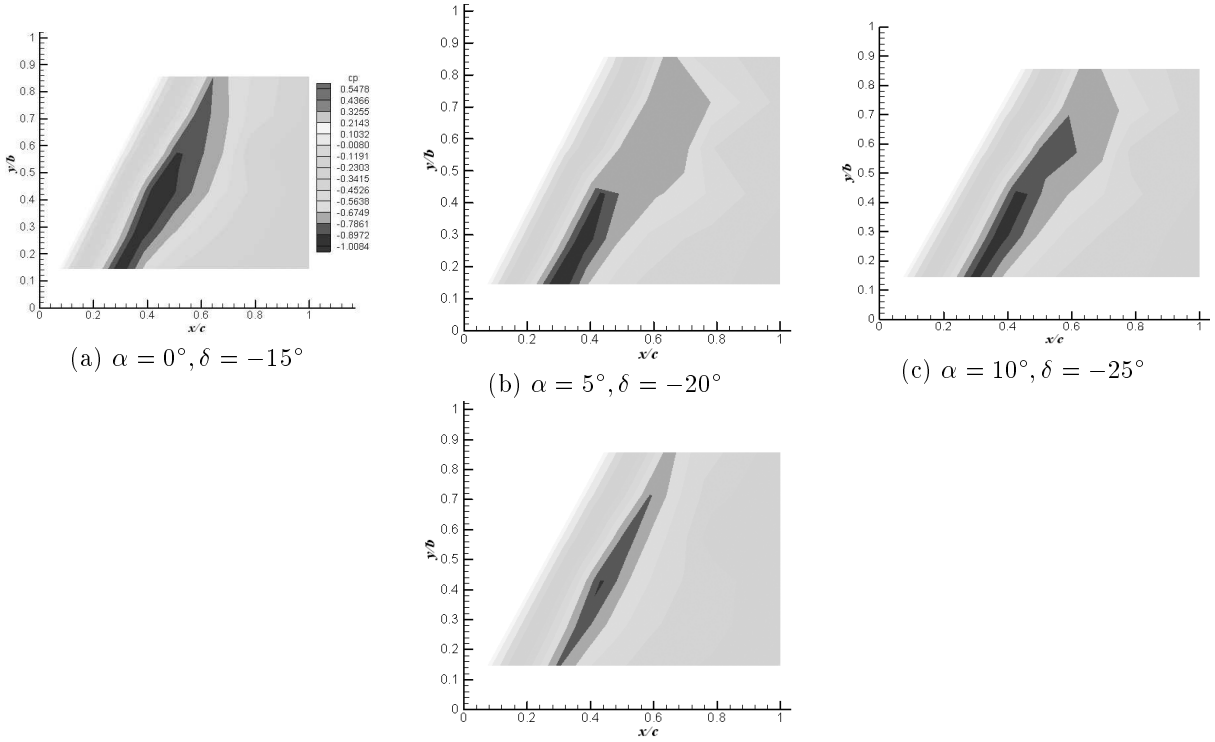

(a) $\alpha = 0°, \delta = -15°$ (b) $\alpha = 5°, \delta = -20°$ (c) $\alpha = 10°, \delta = -25°$

(d) $\alpha = 15°, \delta = -30°$

Figure 11. Tail pressure contours for combinations of body angle of attack and tail deflections for a net inclination of $-15°$.

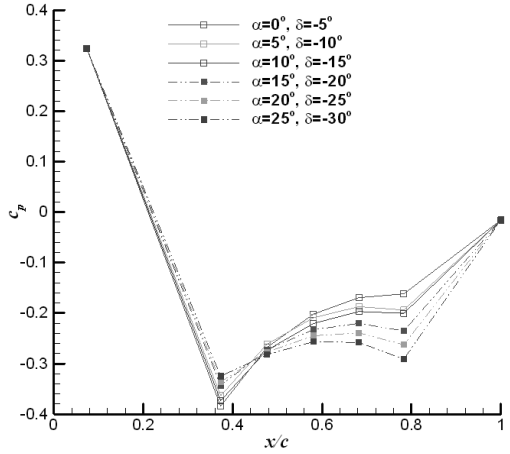

Figure 12. Spanwise tail pressure distribution for combinations of body angle of attack and tail deflections for a net inclination of $-5°(y/b = 0.3)$.

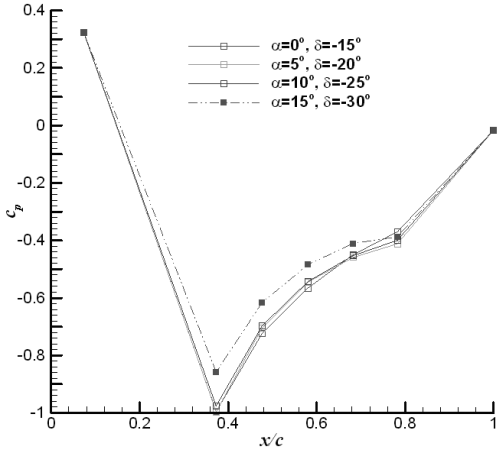

Figure 13. Spanwise tail pressure distribution for combinations of body angle of attack and tail deflections for a net inclination of $-15°(y/b = 0.3)$.

$\delta = 0°$. However, at higher body angles of attack, the flow patterns slightly differ. At high angles of attack, another vortex is seen downstream of the tail vortex, giving rise to the net pressure force on the tail. This effect can be better observed from the chordwise pressure distribution shown in Figure 15. This figure verifies that increasing the body angle of attack is more effective than increasing the tail deflection angle for equal net tail inclination, *i.e.* the combinations "$\alpha = 5°, \delta = 0°$", "$\alpha = 15°, \delta = 5°$" and "$\alpha = 30°, \delta = 5°$" develop a higher suction peak than those of "$\alpha = 0°, \delta = 5°$", "$\alpha = 5°, \delta = 15°$" and "$\alpha = 5°\&\delta = 30°$" respectively. This clearly indicates the favorable effect of nose and body vortices on the flowfield over the tail, especially at moderate to high inclination angles.

In Figure 16, the variation of the tail normal

force with the inclination angle for two cases; zero tail deflection, varying body angle of attack and zero angle of attack, varying tail deflection is shown. As seen from previous figures, at low to moderate deflection angles up to 15 degrees, where the vortex burst onset reaches the tail surface, the normal force developed by the body angle of attack is more than that of the tail deflection. Once the tail vortex started to breakdown on the surface, the body angle of attack, amplifies the adverse effects of the flow separation and the lift due to body angle of attack decreases. For high angles of attack, the nose and forebody vortex shedding give rise to the normal force developed on the tail due to the body angle of attack.

CONCLUSION

A half body-tail combination has been tested in a subsonic wind tunnel to investigate the effects of forebody vortex shedding on the tail surface pressure

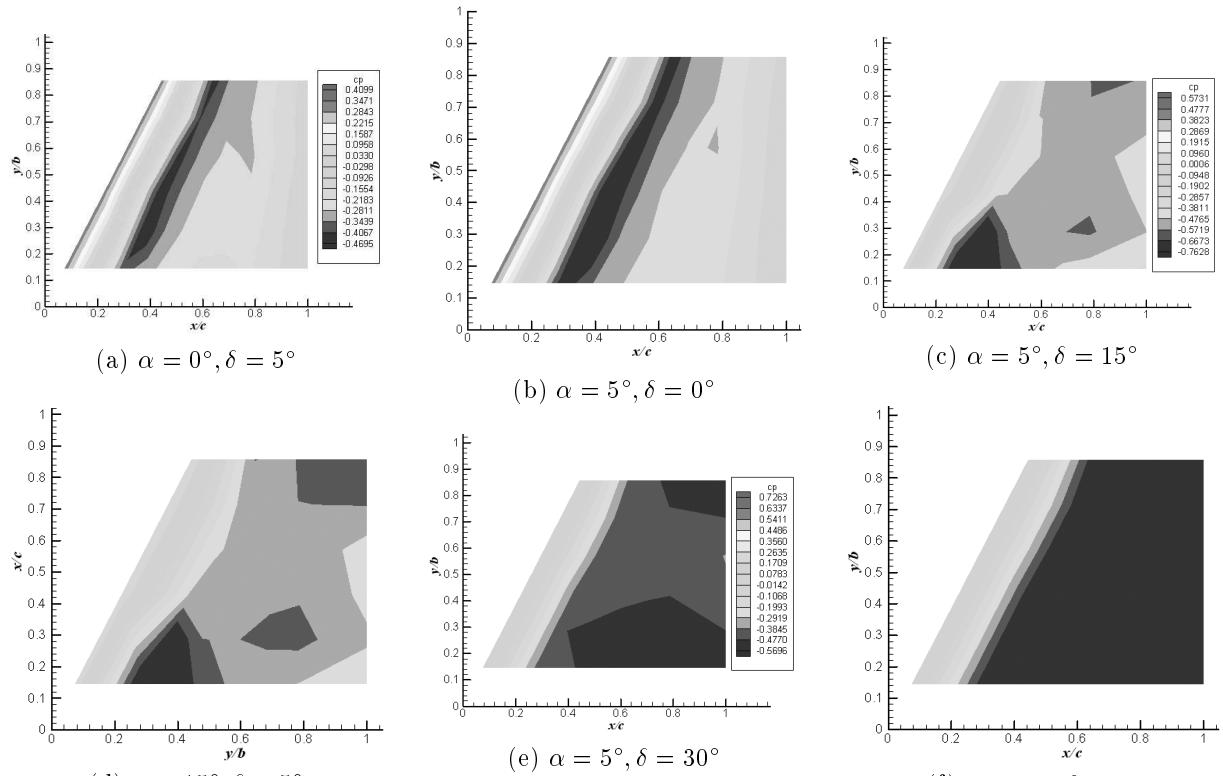

(a) $\alpha = 0°, \delta = 5°$ (b) $\alpha = 5°, \delta = 0°$ (c) $\alpha = 5°, \delta = 15°$

(d) $\alpha = 15°, \delta = 5°$ (e) $\alpha = 5°, \delta = 30°$ (f) $\alpha = 30°, \delta = 5°$

Figure 14. The combinational effects of the body angle of attack and the tail deflection angle.

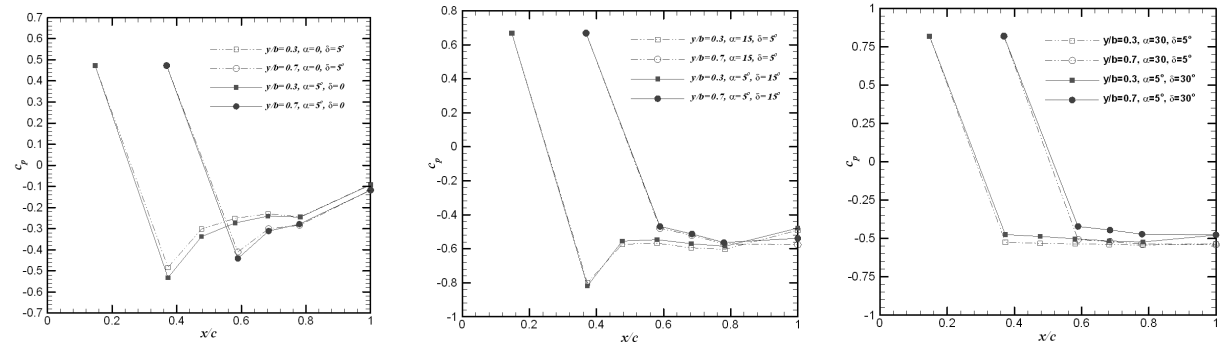

(a) Net tail inclination= 5° (b) Net tail inclination= 10° (c) Net tail inclination= 25°

Figure 15. The combinational effects of the body angle of attack and the tail deflection angle on the spanwise pressure distribution.

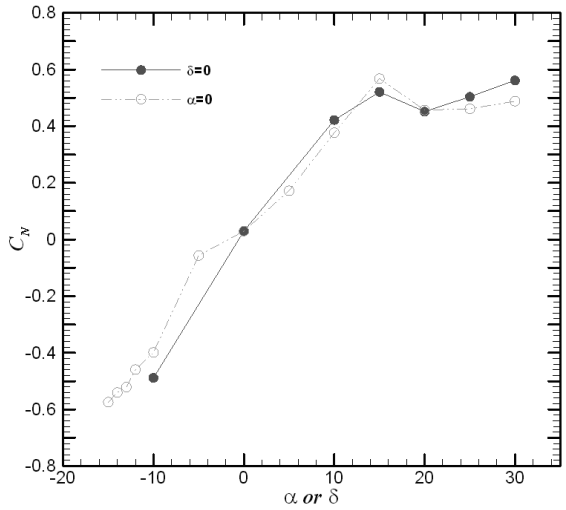

Figure 16. Effects of body angle of attack and tail deflection angle on the normal force of the tail.

pattern. The results show that the body angle of attack, while the relative angle between the body and the tail is zero, is equivalent to the tail deflection for zero body angle of attack, up to tail stall angle. Beyond stall, the vortices shed from the nose and the body seem to be more effective on the tail flow pattern. For the combinations of the body angle of attack and the tail deflection angles, while the net tail inclination with respect to the oncoming flow remains constant, the tail normal force due to the body angle of attack has shown to be more than that developed by the tail deflection.

REFERENCES

1. Schindel L.H., "Effects of Vortex Separation on the Lift Distribution on Bodies of Elliptic Cross Section", *Journal of Aircraft*, **6**, (1969).
2. Bryson A.E., "Symmetric Vortex Separation on Circular Cylinders and Cones", *Journal of Applied Mechanics*, **26**, (1959).
3. Kelly H.R., "The Estimation of Normal Force, Drag, and Pitching Moment Coefficients for Blunt-Based Bodies of Revolution at Large Angles of Attack", *Journal of the Aeronautical Science*, **21**(8), (1954).
4. Grosche F.R., "Wind Tunnel Investigation of the Vortex System Near an Inclined Body of Revolution with and without Wings", *AGARD CP 71*, .
5. , "Dynamic Stability Parameters", *AGARD FDP Lecture Series, AGARD-LS-114*, (1982).
6. , "High-Angle-of-Attack Aerodynamics", *AGARD FDP Lecture Series, AGARD-LS-121*, (1982).
7. Hunt B.L., "Asymmetric Vortex Forces and Wakes on Slender Bodies", *AIAA Paper 82-1336*, (1982).
8. Lamont P.J., "The Complex Asymmetric Flow Over a 3.51D Ogive Nose and Cylindrical Afterbody at High Angles of Attack", *AIAA Paper 82-0053*, (1982).
9. Hemsch M.J., *Tactical Missile Aerodynamics: General Topics*, (1991).
10. Abney E.J., "High Angle of Attack Aerodynamic Predictions Using Missile Datcom", *AIAA Paper 2005-5086*, (2005).
11. Thomas G.B., Roy D.M. and John H.L.V., *Mechanical Measurements*, Addison-Wesley Publishing Company, (1993).